Gulf and Caribbean Research

Volume 27 | Issue 1

2016

Hydrodynamic Variability in a Microtidal Coastal Bay Geographically Susceptible to North East Trade Winds

Israel Medina-Gómez
Centro de Investigación y de Estudios Avanzados del I.P.N. (CINVESTAV-IPN), imedgomez@gmail.com

Cecilia Enríquez
Unidad Multidisciplinaria de Docencia e Investigación (UMDI)

Björn Kjerfve
American University of Sharjah, University City, Sharjah, United Arab Emirates

Ismael Mariño
CINVESTAV-IPN

Jorge Herrera-Silveira
CINVESTAV-IPN

DOI: 10.18785/gcr.2701.06

GULF AND CARIBBEAN

RESEARCH

Volume 27
2016
ISSN: 1528–0470

Published by

THE UNIVERSITY OF
SOUTHERN MISSISSIPPI

GULF COAST RESEARCH LABORATORY
Ocean Springs, Mississippi

Gulf and Caribbean Research Vol 27, 52-65, 2016
DOI: 10.18785/gcr.2701.06
Manuscript received, January 24, 2016; accepted, June 29, 2016

HYDRODYNAMIC VARIABILITY IN A MICROTIDAL COASTAL BAY GEOGRAPHICALLY SUSCEPTIBLE TO NORTH EAST TRADE WINDS

Israel Medina–Gómez[1]*, Cecilia Enríquez[2], Björn Kjerfve[3], Ismael Marino–Tapia[1], and Jorge Herrera–Silveira[1]
*[1]CINVESTAV–IPN, Km. 6 Antigua Carretera a Progreso, Cordemex, C.P. 97310, Mérida, Yucatán, México; [2]UMDI, Puerto de Abrigo s/n, Sisal Hunucmá, Yucatán, C.P. 97355; [3]American University of Sharjah, University City, Sharjah, United Arab Emirates; *Corresponding author, email: imedgomez@gmail.com*

Abstract: The ecological integrity and overall health conditions of natural coastal systems are largely based upon the balance among physical processes. The objective of this study was to assess the effects of tides and winds on the water level variability, circulation patterns, and turnover time in Bahia de la Ascension (BA), a shallow, tropical coastal bay in the Mexican Caribbean prone to the influence of Trade winds due to its geographical location. The analysis of the hydrodynamics of BA using a 2D numerical model indicates that the tidal flow in the inlets and central basin of the bay vary by tidal phase. An averaged seawater inflow through the south inlet and outflow through the north inlet is observed for every simulated case, while peak instantaneous current velocities are evident in the northern entrance. Winds play a dominant role in the water turnover from the system's interior to the main bay. The model shows an average turnover time of 45 days for the whole bay, with shorter turnover when Trade winds impart stress along the main northeast–southwest axis in the bay. Since the tidal signal is attenuated in the southwest endpoint of the bay, the relevance of winds in the transport phenomena was considered fundamental to preserve the ecological heterogeneity of BA.

Keywords: numerical model, residual flow, flushing time, Yucatan Peninsula, western Caribbean.

Introduction

The coastal oceanographic phenomena exert a main control over the hydrology of tropical estuaries, lagoons, and bays. Because of the variable open–boundary nature in these shallow ecosystems coastal hydrodynamics modulates their water exchange with the sea, and consequently, the rate and magnitude of key processes (e.g., salt and nutrient fluxes; Hench et al. 2008). The energy supplied by tides represents a salient forcing controlling the mixing and transport of materials. Even in restricted lagoons subjected to low tidal range, tidal forcing may account for up to 70% of the water level variability, driving a substantial advective, ocean–directed water transport (David and Kjerfve 1998).

However, when tidal range is small, long–term (in the order of months; *e.g.*, seasonal) and short–term (in the order of hours; e.g., winds plus heat balances) meteorological forcing may have a greater influence on the coastal environment than tides (Cavalcante et al. 2011). This non–tidal forcing can induce sea level oscillations with a period greater than a few days in the interior of coastal lagoons, altering net transport. Additionally, the balance between freshwater influx and saltwater incoming from the ocean may force gravitational circulation in estuaries and coastal lagoons, contributing to dissolved and particulate materials transport, as well as dispersion of biota across the seaward boundary (Geyer 1997, Brown et al. 2004).

Since the fluctuating hydrology in semi–enclosed systems is highly dependent on their connectivity to the adjacent shelf sea, changes in the coastal physical setting may have profound ecological implications on them (Drew 2000, Ladah et al. 2012). Thus, a proper grasp of the interplay among physical processes is of primary importance to thoroughly understand the patterns of hydrological variability and asses the overall health condition for such aquatic systems (Nixon 1988, Wolanski 1994, Umgiesser and Neves 2005).

The objective of this study is to explore the dynamic responses of water level, currents, water exchange, and circulation in response to tidal and wind forcing in a shallow, tropical coastal bay using a numerical simulation model. It is hypothesized that, given the microtidal regime in the western Caribbean, the predominant northeast trade winds rather than tidal variability more strongly influences the overall circulation patterns in this ecosystem. We are also interested in examining how the bay's turnover rates respond to the typical wind forcing experienced in the region. Furthermore, given the trend of human–driven disturbance experienced in many semi–enclosed coastal ecosystems and their intrinsic vulnerability, as well as the scarcity of analytical studies to diagnose the responses to the physical–environmental setting in developing countries, the current study is deemed both a timely and relevant effort.

Study Site

Bahia de la Ascension (BA) is a shallow coastal bay of the western Caribbean (Figure 1A), with average depth of 2.3 m and maximum depth of 6.8 m at the north inlet (Figure 1B). The bay's main axis is NE–SW and surface area is 580 km^2, with total mean water volume of 1.33 x 10^9 m^3. The tidal characteristics of this region are mixed, semi–diurnal, microtidal regime (range <0.20 m within the bay), dominated by the principal lunar (M_2) component with amplitude of

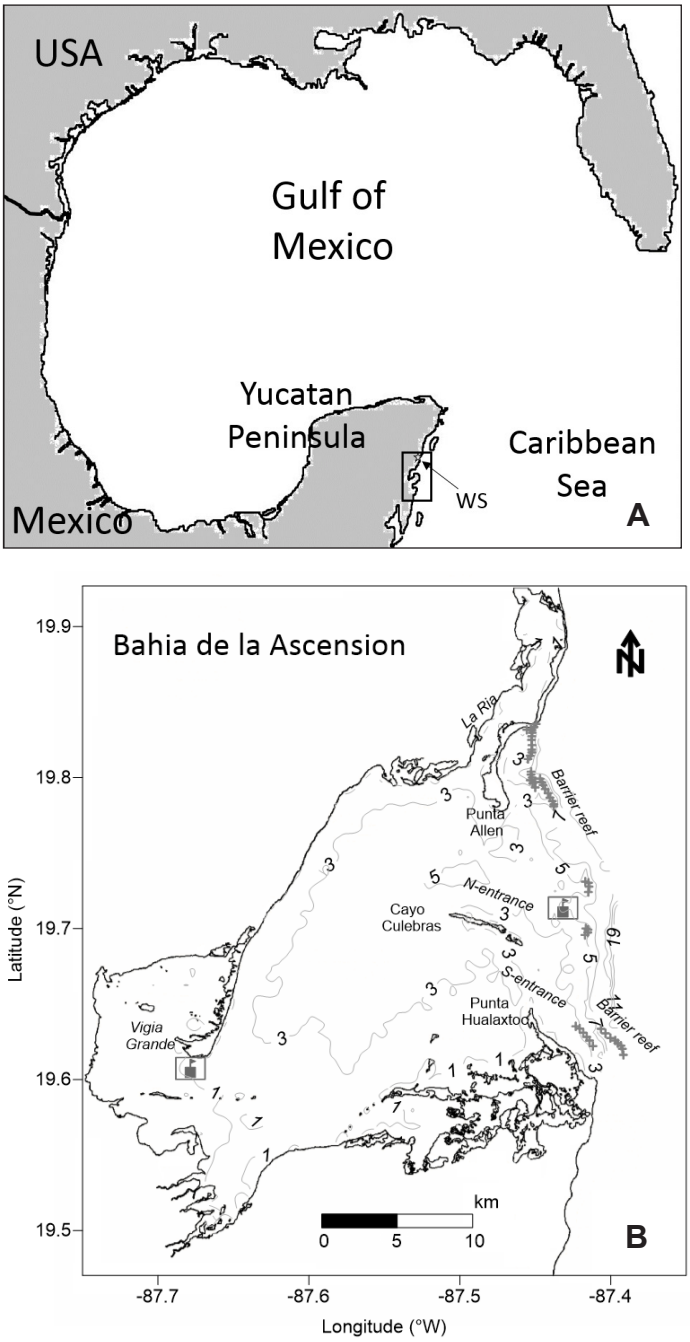

FIGURE 1. Map of the Gulf of Mexico showing Bahia de la Ascension in the Western Caribbean. A. Location of the weather stations northward from the study site (WS). B. Bahia de la Ascension with bathymetry (isobaths in meters) and seaward, discontinuous coral reef formation (x). Grey flags represent moored CTD's in the inner bay and reef lagoon.

0.074 m (Kjerfve 1981) and tidal prism of ≈105 x 10^6 m^3 per semidiurnal cycle. The bay is rimmed seaward by the Mesoamerican Barrier Reef System (MBRS), the world's second largest coral reef formation stretching across four countries (Honduras, Guatemala, Belize, and Mexico).

The ratio between buoyancy forcing (volume of freshwater per tidal cycle) and tidal forcing (tidal prism volume) in the bay is consistent with prevalent vertically homogeneous water column conditions in the inlet zone, with mild vertical stratification in the northern entrance only during peak precipitation periods and less energetic conditions associated with neap tides (Medina–Gómez et al. 2014a). The estimated water residence time in this system during dry and rainy seasons, respectively, is 1,525 days and 203 days (computed according to the freshwater fraction method; Medina–Gómez et al. 2014a). The ratio of groundwater input to tidal prism in BA is nearly 1% in the rainy season and only 0.07% during the dry season.

This system is part of the Sian Ka'an Biosphere reserve (SKBR) in the Yucatan Peninsula (19°40'32.76'' N; 87°32'30.87'' W), one of the largest protected coastal wetlands in Mexico and a UNESCO's World Heritage Site. The SKBR is southward from a burgeoning tourism destination, considered among one of the fastest human population growth regions in Latin America (annual growth rate within 20–25%; Meacham 2007). Because of the karstified (prone to dissolution of the carbonate rock by infiltrating rainwater) landform common to the Yucatan platform, the BA receives significant freshwater input (357 x10^6 m^3/yr) from an extensive array of fissures in the limestone draining a 1,200 km^2 hydrological basin through both diffuse and point sources (*i.e.*, submerged groundwater discharges) venting mainly into the southwest bay. Consequently, SKBR is threatened by the quick development of massive tourism occurring just a few kilometers northward, in the so–called Mayan Riviera.

Marked temporal rainfall heterogeneity rather than temperature variability controls the seasonality of the Mexican Caribbean, featuring a distinct dry season (February–May) and a distinct rainy season (June–October). In addition to the dominant northeast trade winds blowing 32% of the time (mean speed of 3.2 m/s, with strongest winds in June) and southeasterly winds (prevalent in March, with mean speed of 3.3 m/s) in the region, slight precipitation and drop in air temperature associated with boreal winds (i.e., locally known as *Nortes*) occurs from November to January.

Materials and Methods

The spatial variability of water level and currents, estimation of net water discharges across boundaries, and assessment of the time–averaged flow under tidal forcing and different wind condition scenarios were addressed in BA using a barotropic (2D) hydrodynamic model. Also, water level (WL) in the inner bay (Vigia Grande embayment, VG) and the adjacent marine environment (reef lagoon, RL) was recorded during 8 June 2007 (dry season) using an anchored Van Essen Instruments conductivity–temperature–depth recorder (CTD Diver). The WL data series collected in the RL (5 m depth) served to force the model at the ocean end during the validation stage only. On the other hand, the data series obtained in VG (1.5 m) was utilized to compare

the observed versus computed WL values, and further adjust the model parameters during the calibration–validation process. A 10 min sampling rate was set for both moored instruments during 4 days spanning the survey.

Model Setup

A depth–averaged, free–surface hydrodynamic model was implemented using the Delft 3D system (WL–Delft hydraulics) in bi–dimensional mode. The model simulates

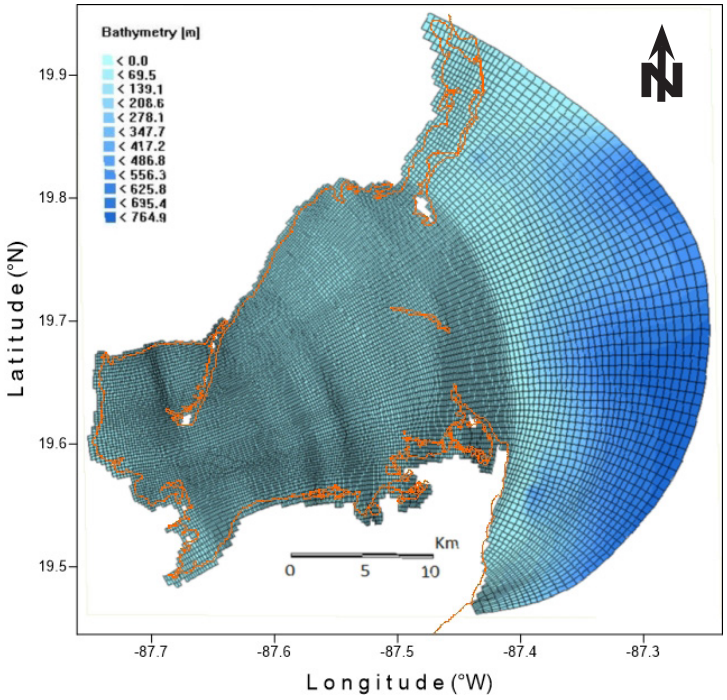

FIGURE 2. Adaptive grid of the model domain

non–steady flow resulting from tidal and meteorological forcing. The space in the computational region was partitioned using a Cartesian, curvilinear, adaptive grid–cell arrangement with 23,200 nodes with spatial resolution varying from 100 m inside the bay (the site of interest), to a coarser horizontal resolution ≈1,000 m on the shelf (Figure 2). Such a grid arrangement allows smooth spatial variation over the model domain minimizing inaccuracy errors in the finite difference operators (WL–Delft hydraulics).

The spatial discretization of the horizontal advection term was undertaken by using the cyclic method, which does not set a restriction in the time step. This flexibility enabled us to implement an alternating direction implicit (ADI) time integration (Delft3D–FLOW). Such a scheme splits one time step into 2 stages and fully solves all shallow water equations on each of such stages by taking a given term (water level gradient, advection) implicitly in time, and further taking the same term explicitly in time in the next stage (i.e., the other half–time).

Thus, from the 3 convergent solutions obtained–all of them achieving numerical stability within 2 semi–diurnal cycles as tested by the system's kinetic energy (Table 3; Medina–Gómez 2011), a Δt = 3 min was selected for the simulations, since this time–step met both numerical stability (Courant number criteria: accuracy in reproducing important spatial length scales and stability for the current barotropic model; WL–Delft hydraulics) and reasonable computational requirements.

The horizontal geometry (wet versus dry) are updated in the model domain every time a new water level is computed. This half–time steps scheme results in an overall second order accuracy in space solution for the integrated time step. The wet–dry framework is based on an algorithm that activates a switch by individually assessing depth values at the cell interfaces. Any time total water depth in a water level point is negative (i.e., dry), that horizontal cell is removed from the computation and the half–time step is repeated. Further, the initial water level at a dry cell is defined by the depth at a given water level point.

To avoid potential boundary effects, a weakly–reflective open boundary (low–pass filter using an alpha–coefficient equal to 0.2; WL–Delft hydraulics) was positioned 15 km seaward from the reef barrier. This distance was set according to the availability of bathymetric data for the region (Cetina et al. 2006).

The turbulence closure model is based on the eddy viscosity concept and defined in the Delft3D–FLOW module for 1–layer (depth–average). According to the Rossby number calculated for the system (3.4 x10^{-5}), deflection of the tidal current towards the right is not negligible given the size of the model domain (e.g., prominent role of rotational processes on the flow field: Ro << 1; Tilburg et al. 2011). Thus, the latitude location of the model area on the Earth's globe was provided to take the Coriolis force into account in the simulation–default in Delft 3D.

Model Calibration and Validation

The model was calibrated by prescribing a 4 day length water level (collected in the reef lagoon; Figure 3) forcing

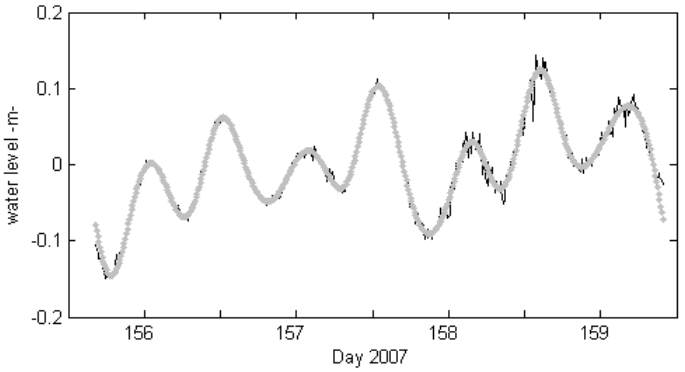

FIGURE 3. Water level in the reef lagoon site (measured, solid black lines; 6-hr low-pass, grey dotted line). High frequency oscillations were eliminated from the raw water-level data by using a discrete Fourier transform filter. This water level was specified at the ocean boundary during calibration-validation of the numeric model.

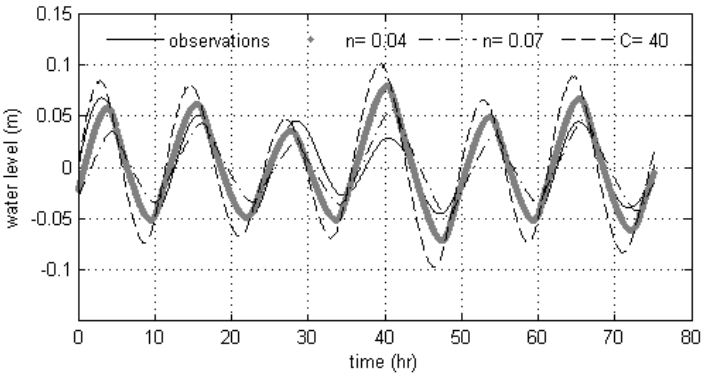

FIGURE 4. Water level at the Vigia Grande mooring (inner-most bay). Observations (demeaned time series) compared with simulated data obtained through different bottom roughness formulae: Chezy coefficient, C = 40 $m^{1/2}/s$ and two Manning coefficients, n = 0.04 and 0.07 (independent of units).

in the ocean end and further adjusting the bottom friction coefficient until reaching a water level close to that observed in the inner bay (Figure 4). We considered it appropriate to carry out the calibration–validation phase simulations using the reef lagoon and inner–bay water levels, since both time–series were obtained at the same period of time and influenced by identical background processes such as wind stress, tidal phase, and prevalent atmospheric conditions.

Since deep water is found beyond the reef crest (Figure 2), it seemed reasonable to assume a lack of shoaling on the tidal wave prescribed at the seaward boundary before stepping into the bay's edge (e.g., reef lagoon). Nonetheless, we accounted for the phase–shift presumably experienced by the water level signal across the 18 km distance (15 km from the seaward edge of the model domain to the reef crest plus 3 km from the reef crest to the mooring site within the reef lagoon) between the ocean boundary (where the forcing was prescribed) and the mooring site onto the reef lagoon (where the time series was actually recorded), by computing the phase lag of the M_2 tidal frequency (the most influential harmonic constituent in this region; Kjerve 1981) between the outer bay (Reef Lagoon) and inner–bay (Vigia Grande). The distance between the Vigia Grande and Reef Lagoon moorings is roughly 22 km, or a distance ratio between ocean boundary–reef lagoon to reef lagoon–inner bay segments equal to 0.82.

The harmonic analysis using T_TIDE showed that the M_2 tidal constituent lagged ≈1.12 h (32.24°) behind in the inner bay relative to the reef lagoon (Pawlowicz et al. 2002). By considering the distance ratio between segments, a lag of > 55 min was estimated between the ocean boundary and the reef lagoon. Consequently, a phase shift of 1 h was implemented for every modeled water level (i.e., those produced by distinct bottom roughness coefficients) before proceeding with fitting between observed and modeled water level time series.

A Chezy coefficient (default in Delft) of C = 40 $m^{1/2}/s$ and two different Manning roughness coefficients of n = 0.04 and 0.07 (independent of units) were applied in the simulations during the calibration–validation phase. Such roughness values are within those reported for macrophyte–dominated habitats (e.g., 0.03–0.30; Dawson and Robinson 1984) and have been utilized in studies to parameterize bottom friction in shallow ecosystems colonized by aquatic vegetation (e.g., 0.02–0.20; Morin et al. 2000).

After removing the first day (2 semidiurnal cycles) from startup at every simulation for stabilization reasons, the agreement between modeled and measured water level was quantified utilizing the root–mean square error (RMSE; eq. 1) and the relative mean absolute error (RMAE; eq. 2). Both statistics are widely used to evaluate accuracy of numerical models (Fernandes et al. 2001, Sousa and Dias 2007, Walstra et al. 2001):

$$\text{Eq. (1)} \quad \text{RMSE} = \sqrt{\frac{1}{N}\sum_{n=1}^{N}[x_{OBS} - x_{MOD}]^2}$$

$$\text{Eq. (2)} \quad \text{RMAE} = \frac{\frac{1}{N}\sum_{n=1}^{N}(X_{MOD} - X_{OBS})}{\frac{1}{N}\sum_{n=1}^{N}\langle X_{OBS}\rangle}$$

where X_{OBS} and X_{MOD} are the set of N observed and modeled values, respectively.

The minimum difference between the observed water level and that predicted by the model at the inner bay corresponded to a Manning coefficient equal to 0.04, yielding RMAE ≈ 0.17 (Table 1). According to the error categorization provided by Sutherland et al. (2004), RMAE values < 0.2 are qualified as an excellent match between predictions and observations.

TABLE 1. *Statistics summarizing the model performance. Root Mean Square Error (RMSE); Relative Mean Absolute Error (RMAE). n = 501.*

Bottom friction formulae	RMSE (m)	RMAE *
Chezy, C= 40 $m^{1/2}/s$	0.0239	0.6531
Manning, n = 0.04	0. 0228	0.1664
Manning, n = 0.07	0.0234	0.2316

*Values <0.2 correspond to an excellent agreement (Sutherland et al. 2004).

Additionally, harmonic constants of the tidal constituents for the observed and modeled water level time series were calculated for comparison. The correlation coefficients among observed versus modeled tidal constants (Table 2) differ from the statistics computed from the actual water level data series, as Chezy's is better qualified (amplitude correlation = 0.99, p ≈ 0; phase correlation = 0.86, p = 0.007) than the Manning formulae (amplitude correlation

TABLE 2. *Harmonic constants of tidal constituents (amplitude and phase) for both observed and modeled (applying distinct bottom friction coefficients) water level time-series at an observation point in the inner-most bay. Amp—amplitude; Pha—phase; Obs—observed; M04 and M07—Manning roughness coefficients of n = 0.04 and n = 0.07, respectively; Chez—Chezy modeled coefficients.*

Tide	Frequency (cph)	Amp_Obs	Pha_Obs	Amp_M04	Pha_M04	Amp_M07	Pha_M07	Amp_Chez	Pha_Chez
K1	0.0418	0.0043	141.53	0.0126	255.37	0.0105	272.74	0.0143	240.47
M2	0.0805	0.0479	108.13	0.0546	99.88	0.0353	119.77	0.0775	80.58
M3	0.1208	0.0028	2.51	0.0036	34.83	0.0026	47.88	0.0046	24.13
M4	0.1610	0.0011	155.58	0.0009	181.8	0.001	223.45	0.0004	233.7
2MK5	0.2028	0.0005	201.8	0.0009	107.68	0.0011	166.41	0.0001	206.48
M6	0.2415	0.0005	160.01	0.003	324.77	0.0024	14.42	0.0016	269.04
3MK7	0.2833	0.0002	206.52	0.0005	151.48	0.0006	203.32	0.0003	267.4
M8	0.3221	0.0003	167.28	0.0001	341	0.0002	172.29	0.0006	197.19

= 0.98, p ≈ 0; phase correlation = 0.46, p = 0.25). However, the correlation coefficient has been reported as a poor parameter quantifying accuracy of forecasts produced by numerical systems (Murphy 1988). These results led us to consider that n = 0.04 yielded the best fit between observed and simulated tidal ranges.

Hydrodynamic Simulation Scenarios

For all the numerical simulations scenarios the model was forced at the open boundary with a water level time series reconstructed from tidal components (M_2, S_2, N_2, K_1, O_1, P_1) reported for Cozumel Island, located 60 km north from BA (Kjerfve 1981). Besides applying a spatially uniform n bottom friction parameter, other predefined initial and boundary conditions were background water salinity equal to 35 and temperature of 28°C. Also, water level forcing at the offshore boundary was set to begin with the rising phase (zero—level in the water column at the start time of the simulation) of such a reconstructed signal from local tidal constituents (Kjerfve 1981). The first day of the simulation time (2 semi—diurnal cycles spin—up) was further removed from the simulation results prior to analysis (Table 1). No freshwater input was included in the set of boundary conditions of this model.

Along with a tidally forced stand—alone case, a series of simulations comprising identical tides plus 3 regionally typical wind conditions were executed: 1) Northeasterlies (Trade winds); 2) Southeasterly winds; and 3) Northwest—North winds (*Nortes*). Wind data were provided by the National Meteorological Service (SMN) from a weather station (Forest Technology Systems, Ltd.) located 9 m above the ground and 38 km northward from BA (Figure 1a), within the Sian Ka'an Biosphere Reserve (SMN 2007).

The 3 wind events were simulated using real, time—varying, spatially homogenous data with a 10 min sampling frequency rather than prescribing artificial, steady winds (Figure 5). We believe this approach allows elucidating the ecosystem's hydrodynamic response to the most prevalent local wind scenarios under real conditions as much as possible. Otherwise, using unidirectional/constant velocity wind data sets may overestimate the wind stress influence on water circulation, whilst time—varying responses of hydrodynamics in semi—enclosed ecosystems to short—term processes (e.g., seiches) might be overlooked (Staneva and Stanev 1998, Enriquez et al. 2010).

Wind events were selected by ensuring that every data series involved both a minimum direction persistence over an 8 d period and relatively high velocities according to the mean values reported for this zone. The specified duration for simulations is tied to the characteristic duration of *Nortes* (i.e., winds from the N and NW associated with polar high—pressure fronts featuring low air temperature), which are characteristically short—lived episodes in the Yucatan

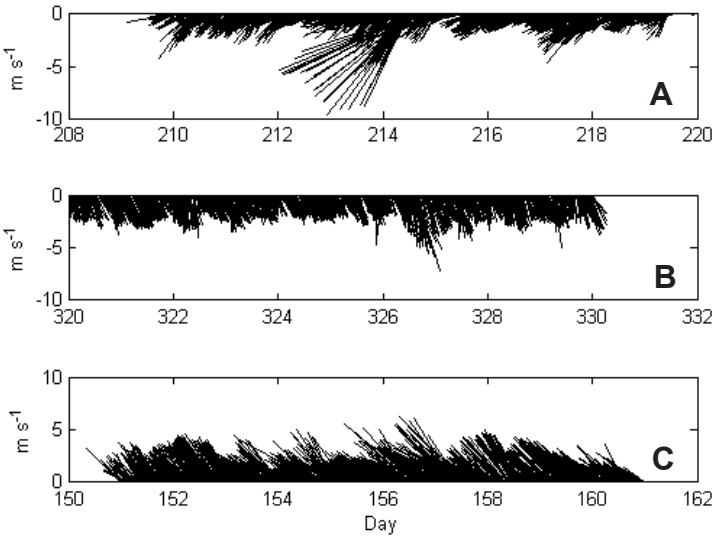

FIGURE 5. Three wind events occurring in 2007 and utilized in combination with tides to force the hydrodynamic model. A. Trade winds. B. North winds. C. Southeast winds.

TABLE 3. *Summary of the numerical simulations. ST—spring tide.*

Modeling stage	Cases	Forcing functions	Simulation time (days)	Observations
Stability tests	Kinetic energy	M_2 tide	10	Three Δt's tested: 1, 3, and 9 min
	Volume conservation	M_2 tide	30	Experiment carried out with Δt = 3 min
Reliability tests[a]	Calibration and Validation	4 day-length surface elevation observations	4	Time series collected in the reef lagoon was prescribed at the ocean end for calibration. The validation was performed by comparing bottom roughness formulae and inspecting the best fit between observed and modeled tidal ranges in a fixed point of the bay's interior
Hydrodynamic simulations[a]	Tides and winds	ST + northeasterly winds ST + southeast wind ST + "Nortes" (N-NW)	8	ST plus real winds. Wind data uniformly distributed across the model domain. Water level specified at the open boundary was a reconstructed time series from local tidal constituents recorded 60 km north of BA[b]

[a]First 24 h from startup (2 semi-diurnal cycles) were removed due to stability reasons.
[b]Kjerfve 1981.

Peninsula. It is thought that by keeping a standard simulation time, the comparison of model results obtained along distinct cases would be more duly accomplished. The tidal cycles were centered at the midpoint of each 8 d simulation run. The scenarios modeled are summarized in Table 3.

Turnover Time

The turnover time (T_t) was calculated using the rate of water exchange provided by a variety of combined scenarios: spring tides (ST) plus three typical wind events experienced in the region ("suestes", SE; trade winds, NE; "nortes", N—NW). For this purpose, the total time integral of hydrodynamic flows (e.g., the output of the Delft model "instantaneous water discharge" given in m^3/sec) through the bay—shelf boundary at both inlets (north and south entrances; Figure 1b) during one day were computed for each of the combined boundary conditions simulated (Q), and then the volume of the system (V; assumed to be constant during the simulation time and completely mixed on a time scale shorter than the turnover time; Kjerfve and Magill 1989) was divided by the integrated rate of water exchange between the bay and the ocean. T_t is given in days:

$$\text{Eq. (3)} \qquad T_t = V/Q$$

Results

The relative impact exerted by the assessed forcing functions on Bahia de la Ascension circulation is a consequence of the spatial and temporal scales under scope and the local geomorphologic features across the bay. Thus, the tidal energy input leads to strong instantaneous currents in the inlet areas and near the channel connecting the main bay with the southwestern embayment (Vigia Grande). Furthermore, sub—tidal events (e.g., Trade northeasterlies) drove a large residual, ocean—directed flow in the bay.

Instantaneous Currents

The instantaneous currents observed in BA when tidal input is the only forcing showed a seaward water motion under ebb tide through both inlets, yet stronger currents and a smoother water level transition zone were evident across the north entrance during ebbing compared to the southern inlet (Figure 6A). Also, swift currents occurred at the southern subsystems indicated a rapid emptying of these inner embayments. During low water, relatively slow incoming water masses observed in the inlets contrasted with strong water motion crossing from the SW subsystem Vigia Grande to the main bay. The contact between these opposite—directed currents defined a slight frontal zone along the mid—bay (Figure 6B).

The currents in flood tide indicated water inflow in the inlet zones that extends farther into the bay, although current velocities rapidly decelerated once they reached the central basin. Also, two contrary instantaneous currents coexisted in the channel connecting Vigia Grande and the main bay, with water flowing seaward in the northern portion of the channel and landward water motion occurring across the southern portion of this entrance (Figure 6C). A relatively strong landward current velocity replaced this lateral flow structure further during high water (Figure 6D).

When southeasterly winds were included into the model during the ebbing case, a similar pattern in terms of current direction to the ebb tide alone case was found (Figure 7A). However, the relative magnitude of instantaneous water motion is dampened at the inlets and in the south and southwest inner embayments compared to currents in the central basin, which remain almost unaffected. This variation is particularly evident in the Vigia Grande subsystem, where reduced water outflow led to a steeper water level gradient towards the landward side of the channel compared to the tides stand—alone scenario (Figures 6A and 7A). The phase

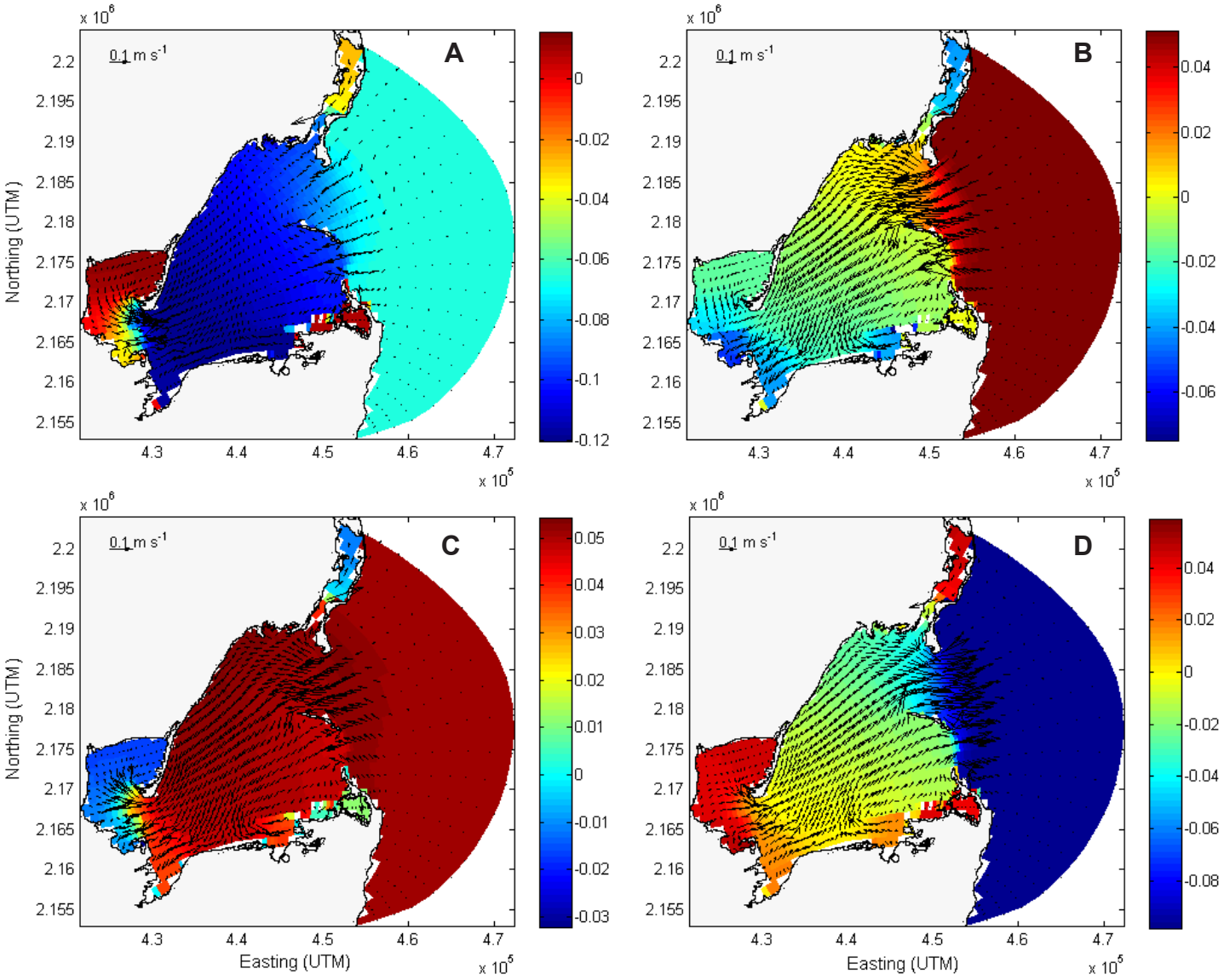

FIGURE 6. Instantaneous water level (m; vertical color bar to the right of the figure) and currents (depth averaged velocity, m/s; vectors) when the model is forced only with tides during 4 instantaneous tidal phases. A. Ebb tide. B. Low tide. C. Flood tide. D. High tide.

shift in the Vigia Grande embayment (Figure 8) reflects the attenuation of the tidal wave as it propagates from the central basin (3 m mean depth) to the shallow inner bay water column (mean depth of 0.5 m).

The circulation under "Nortes" and flood tide is similar to the lack of winds flooding scenario, although current velocities are diminished overall throughout the system, except for the northern section of the bay. The Trade winds plus spring tides case showed an intense flow emptying the SW inner embayment (e.g., towards the central bay) under low tide. During the flood tide plus Trades combined case, water motion is also comparable to the stand—alone tides scenario, with an overall even distribution of the water current velocities throughout the bay (Figures 7C and 7D).

Residual Currents

The tide averaged currents over 14 semidiurnal cycles (*i.e.*, first day removed from the 8 d simulation run for numerical stability) simulated under the effect of astronomical tides alone showed incoming flow along "Cayo Culebras" mangrove cay (CC) in the inlet zone, with strong flow in the western tip of the cay (Figure 9A). Because of the tidal energy dampening just past the channel into the VG embayment (Figure 8), the net tidal flow in the VG embayment is minor and limited to the channel between this inner subsystem and the central basin (Figure 9A).

The circulation pattern occurring under southeasterly winds plus spring tides resulted in a predominantly northward residual flow parallel to the reef barrier (mean velocity of 0.04 ± 0.02 SD m/s and 0.12 m/s maxima), which caused a bay—directed transport through the south inlet (Figure 9B). Pervasive SE wind sustained a clockwise cell (radius ≈ 5 km) flowing in the southern portion of the central basin, in front of the connecting channel with the SW embayment Vigia Grande (Figure 9B).

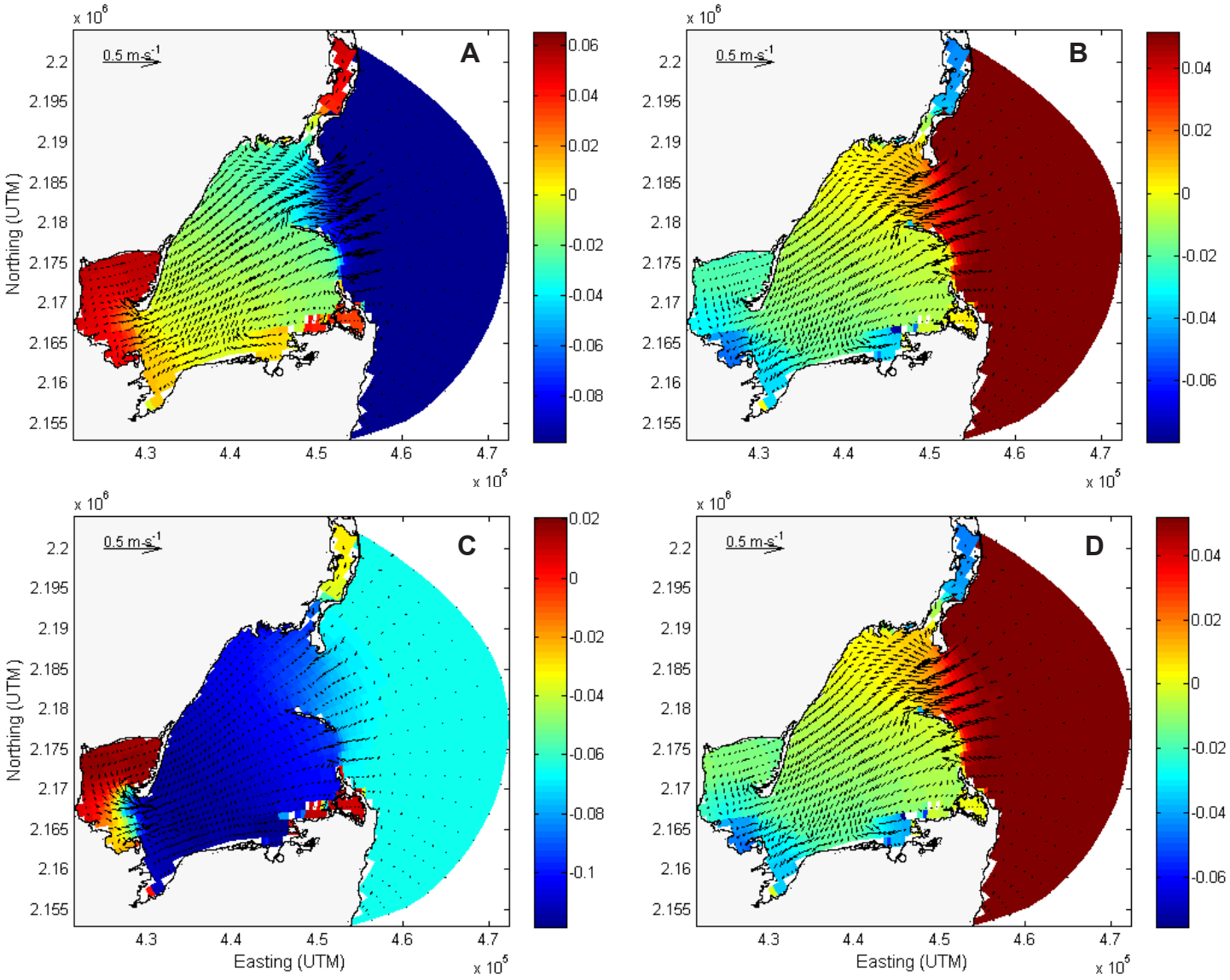

FIGURE 7. Instantaneous water level (m; vertical color bar to the right of the figure) and currents (depth averaged velocity, m/s; vectors) when the model is forced with tides plus winds. A. Southeast winds in ebb tide. B. "Nortes" winds in flood tide. C. Trade winds in low tide. D. Trade winds in flood tide.

The simulation results obtained with the combined NW–N wind field (i.e., "Nortes") and spring tide forcing exhibited an active alongshore and southward water transport with peak current velocity of 0.03 m/s. The water exited the system through the north entrance. Also, an anticlockwise cell circulation was observed close to the one occurring under SE winds (Figure 9C).

During the Trade wind event, a prevalent southward coastal flow with peak current velocity of nearly 0.05 m/s was observed. The residual current field showed a series of strong currents radiating from the CC cay towards the NW (0.013 m/s), W (0.012 m/s), and SE (0.03 m/s). Trade winds (NE) generated an average current velocity of 0.005 ± 0.003 SD m/s within the bay. A clockwise cell of shorter length scale than those established under SE and NW–N winds took place in the southeast portion of the central basin (Figure 9D). Maximum southeasterly wind–induced currents were only one half of that observed in the Trade winds case.

Both time averaged circulations involving eastern compo-

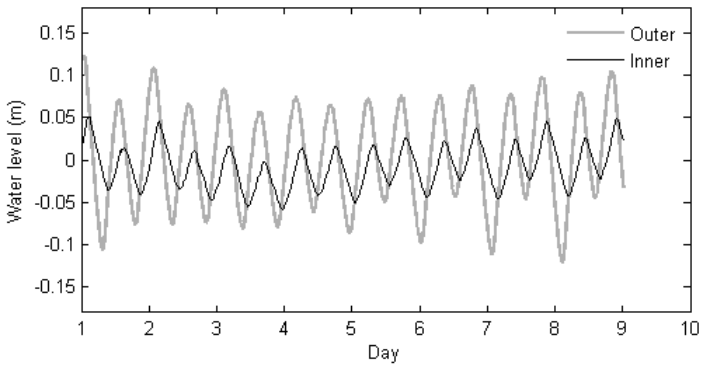

FIGURE 8. Modeled water level obtained in both sides of the channel connecting Vigia Grande embayment (Inner) with the bay's central basin (Outer) under spring tides-southeast winds combined scenario (such conditions are akin to those observed during the June survey).

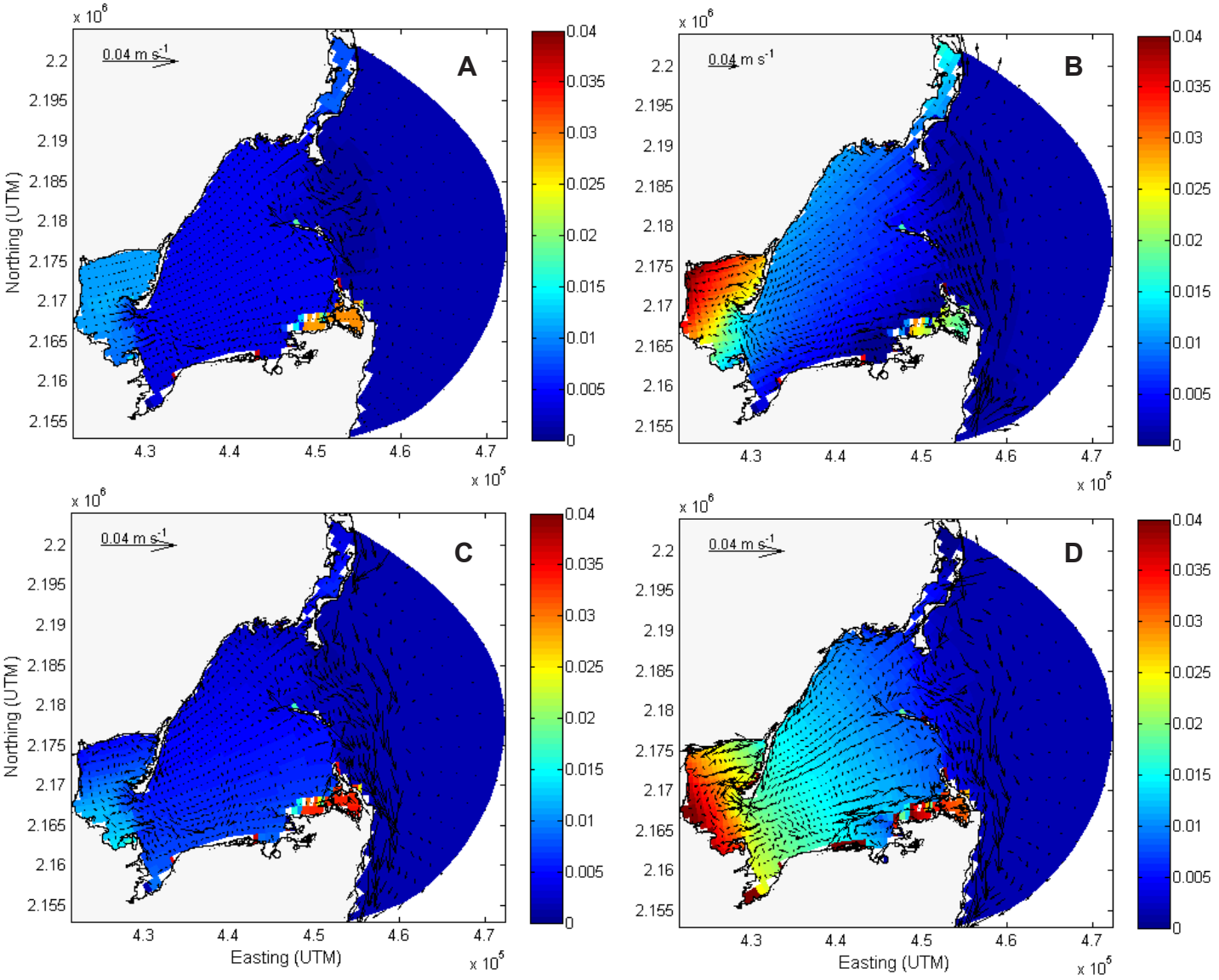

FIGURE 9. Four scenarios of 7 d average water level (m; vertical color bar to the right of the figure) and residual currents (depth averaged velocity, m/s; vectors). A. Tides alone. B. Tides plus southeast wind. C. Tides plus "Nortes" event. D. Tides plus Trade winds.

nent winds (SE wind and NE Trades combined with spring tides) induced a ≈3.5 cm water level increase in the inner–most bay. However, the water level gradient simulated under the Trade winds case showed a smoother spatial distribution along the NE–SW plane of the system than that defined by the southeasterly forcing winds (Figures 9B and 9D). The time–varying water level response within VG embayment during Trade Winds simulation exhibited a water column elevation spanning ≈ 6 hours (Figure 10).

Turnover Time

The turnover times (T_t) showed a pattern seemingly associated with the wind direction, with a mean T_t of 1.5 months for the simulated scenarios. Longer T_t in the whole bay corresponded to the spring tide (ST) stand–alone forcing, as well as under the ST plus "Nortes" event, whilst northeasterly winds (Trades) acting over the BA area drove high water volumes flushing out from the system. For instance, NE Trade winds were responsible for carrying away 387 m^3/d from the system, or nearly 6% more water than either the ST stand–alone forcing or the ST–Nortes combined simulations. As a consequence, Trade winds induced the shortest T_t of the

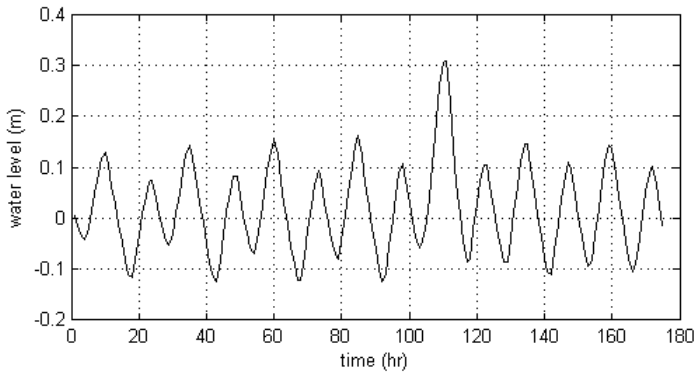

FIGURE 10. Time varying water level (m) in the inner-most bay (Vigia Grande subsystem) during Trade winds simulation.

study (≈42 days), which is 3 days shorter than any other simulated scenario.

Discussion

The simulation of the water circulation in Bahia de la Ascension under the dynamic forcing of tides and 3 typical wind conditions occurring in the Mexican Caribbean showed that, despite a microtidal regime characterizing the area, tides influence the water transport across the inlets. Strong currents with peak velocity of 0.25 m/s corresponded to the northern entrance near the seaward endpoint of the "Cayo Culebras" mangrove cay during spring tides. Nevertheless, tidally—driven effects are mostly confined to the inlet zone and partially across the main bay, as tidal currents substantially decelerate in the upper reaches of the central basin.

Wind stress alters the tidally—driven water movement in BA, as hydraulic flows often defined parallel trajectories to those of winds acting upon the system. The wind influence was more vividly illustrated at the inner—most bay (Vigia Grande embayment) when the model is forced with NE winds. The regional climatologic forcing may represent a main driver of the replenishing time of water in this inner section of the bay. Such a water exchange may be enhanced by the wind—driven setup in the northwest portion of the VG embayment (see Figure 10). However, this modeled water setup induced by the Trade winds is still lower than the 18 cm water level slope reported by Medina—Gomez et al. (2014a) in the inner bay during 5 days of sustained southeasterly winds.

The circulation—constrained SW embayment is the receiving water body of substantial freshwater and abundant materials (e.g., nutrients, dissolved organic matter) draining low—lying, well—developed mangrove forests (Medina—Gómez et al. 2014a). It seems feasible that, due to tidal energy attenuation in the inner bay (see Figure 8), a variable extent of isolation between this inner section and the main bay would occur, unless there is a mechanism controlling the water motion. The easterlies and particularly, the Trade winds, may represent such a wind—driven propagation mechanism of water properties farther into the sea—influenced central basin.

The potential of Trade winds to play a prominent role in the water transport from the bay's interior to the main bay steams from the fact that northeasterly winds act over the bay's surface in the same direction as the system's main axis (i.e., NE—SW), optimizing its forcing effect over the bay's surface and thus, on the water level field. However, this scenario might reduce, at some point, water transport from the main bay into VG during episodes of sustained NE winds, unless a return flow mechanism (e.g., through the bottom layer) is established to maintain a water exchange with the central basin (Kjerfve and Oliveira 2004). Consequently, the water level rise observed in the landward edge of VG (see Figure 9d) might be adjusted through an upwind—directed flow established at depth (Kjerfve and Magill 1989).

It is thought that, in combination with mid—term hydrometeorological process controlling the net freshwater input (Thattai et al. 2003), Trade winds would help to regulate the confinement degree in the inner—most bay and favor the connection between this mesohaline area and the central basin, as well as to spread the hydrographic properties characterizing the southwestern—most subsystem (i.e., Vigia Grande embayment) farther into the bay during episodes of persistent NE winds. If true, this wind—enhanced hydrodynamic feature has the potential to not only alter a number of physical—environmental traits in the whole system, such as thermohaline characteristics in the water column and heat fluxes, but also would lessen the average turnover time in the bay, thus contributing to avoidance of environmental impairment often experienced in locations with constrained circulation (Cavalcante et al. 2012).

The model results indicated that the *Nortes* wind (i.e., N—NW) does not play as relevant a role in the circulation pattern of this bay as in coastal ecosystems of the Yucatan north coast. The northern polar cold—fronts constitute dominant hydrometeorological processes in the northern Yucatan, inducing a remarkable marine influence on its ecosystems and longer water residence times during the winter season which features such events (Medina—Gómez and Herrera—Silveira 2009). Because *Nortes* winds show a trajectory "from the continent" in Bahia de la Ascension instead of "from the ocean" as in the Yucatan north coast, the geographic location of the bay contributes to relieving the potential effects of these events over the system.

The turnover time (T_t) during *Nortes* winds is consistent with a lessened influence on the system hydrodynamics under these events, as nearly the same T_t were calculated both under stand—alone spring tides and *Nortes* plus spring tides scenarios. Also, the mean T_t of 1.5 months calculated in this study is well below the range of previous seasonal turnover time estimations (203—1,525 days in rainy and dry seasons, respectively) carried out in BA using bulk hydro—meteorological information (Medina—Gómez et al. 2014a).

These ample differences between T_t reported elsewhere and that obtained in the current numerical study may reflect an intrinsic methodological variation due to distinct approaches utilized. The water flows of empirical—based Schreiber models (e.g., groundwater discharge, evapotranspiration) used to compute the turnover time (freshwater fraction method) by Medina—Gómez et al. (2014a) occurs at larger time—scales (e.g., seasonal) than both the unidirectional (advective) and three—dimensional (diffusive) water motion (e.g., within hours) accounted for in the processes implemented in this hydrodynamic model (Delft3D).

However, T_t values in BA were much higher than the aver-

TABLE 4. *Geomorphologic and water budget features in four coastal lagoons along the Mexican Caribbean and the Gulf of Mexico (northern and southern regions).*

System	Area (km^2)	Volume ($x\ 10^6\ m^3$)	Depth (m)	Tidal Range (m)	Freshwater Discharge ($x10^6\ m^3/yr$)	Turnover Time (days)
Lake Pontchartrain[a]	1,630	6,031	3.7	0.1	5,929	20-105
Terminos Lagoon[b]	2,500	8,750	3.5	0.4	12,600	67
Puerto Morelos (reef lagoon)	7.5	8[c]	3[c]	0.17[c]	60.2[d]	0.125[c]
Bahia de la Ascension[e]	580	1,422	2.2	0.18	870	45

[a]Kjerfve 1986.

[b]David 1999.

[c]Coronado et al. 2007.

[d]Estimated as fresh groundwater discharge (GD) using the figure provided by Hanshaw and Back (1980) for mean GD in the eastern Yucatan Peninsula equal to 8.6 x106 m3 per year per kilometer of coastline.

[e]Medina et al. 2014a. Except for the turnover time which was computed from the hydrodynamic simulations results in the current study.

age T_t value of 3 h reported for Puerto Morelos reef lagoon (PMRL), located 130 km northward from this study site (Coronado et al. 2007). The PMRL estimation corresponded to typical wave—wind conditions and background current velocity. In addition to striking geomorphologic differences between BA (juxtaposition of a wide, relatively deep and open central basin and a shallow, inner, confined subsystem in the SW extreme, with a well—developed fringing mangrove forest) and PMRL (a relatively shallow reef lagoon bounded by an almost continuous reef barrier seaward and shore coastline landward), PMRL drains relatively higher volumes from a much smaller system (volume of 8 $x10^6$ m^3 with a system transport equal to 986 m^3/s; Coronado et al. 2007) than Bahia de la Ascension (volume of 1,422 $x10^6$ m^3 and system transport of 370 m^3/s; Table 4).

The interplay between such geomorphologic water balance traits may explain the relatively high short—term sensitivity of turnover times in PMRL to a hurricane (T_t = 0.35 h, more than 8 times shorter than the average T_t under a regular physical setting; Coronado et al. 2007) compared to both seasonal (Medina—Gómez et al. 2014a) and climatologic event—driven flushing rates observed in BA. In addition to the previously mentioned return flow, the flooding pattern over adjacent wetland vegetation in BA may also offset water level rise in the landward section of VG generated either by tidal or climatic forcing.

It is thought that because of the low—lying topography in the south and southwestern part of the bay (Adame et al. 2013), even small water level increases lead to the flooding of a vast area featuring an anastomosing network of tidal creeks and sloughs within the adjacent mangrove wetland (Hsu et al. 2013). This flooding regime of the neighboring ecosystems may buffer the hydrodynamic coupling between inner and main bay, defining significant differences from other tropical coastal ecosystems, like in the reef lagoons, where hydrodynamic features are typically associated with both the complex geometry and bottom roughness of reef formations (Lambrechts et al. 2008, Taebi et al. 2011).

Such a vegetation—modulated response adds to the overall system resilience by reducing the impact that strong storms, characteristic of this region (Boose et al. 2003), may exert on the hydrographic heterogeneity and habitat diversity in BA. Flushing times in Terminos Lagoon (David 1999) and Lake Pontchartrain (Kjerve 1986), two restricted lagoons in the Gulf of Mexico significantly larger than BA, exhibited comparable T_t values to BA, despite both aquatic ecosystems being fed by rivers, as opposed to the ground freshwater input in BA (Table 4).

The openness of BA not only controls how shelf sea processes are conveyed into the bay across the inlets, but may also influence the system's sensitivity to variations in the rate and magnitude of atmospheric processes (e.g., strong storms). For instance, homogeneous salinity in Lake Pontchartrain, a brackish system associated with the Mississippi River, reflects both the prominent freshwater input and relatively restricted hydraulic exchange (Kjerfve 1986). Strong salinity changes have been documented in Lake Pontchartrain after water diversion from the Mississippi River into this system to relieve high water levels in the New Orleans rivers following extremely high precipitation (Kjerfve 1986). In contrast, a consistent estuarine gradient was observed in BA throughout the year (seasonal salinity variation < 4), and this horizontal salinity structure was maintained < 2 months after a category 5 hurricane made landfall in the region (Medina—Gómez et al. 2014a). These contrasting patterns suggest a higher vulnerability of the riverine—influenced Lake Pontchartrain than in BA under high intensity events (e.g., hurricanes).

However, the gravitational circulation brought about by

the freshwater supply in the fluvial systems (e.g., inner estuaries) surrounding the landward margin of Terminos Lagoon (Medina—Gómez et al. 2014b) may account for the comparable turnover times between this system and BA, regardless of the significant differences in geomorphologic features between both lagoons (Table 4). The marked seasonal pattern of net freshwater input may exert a mid—term control on the thermohaline circulation of the bay, particularly during the moment of wind—direction change and at the onset of neap tides.

Although only a weak vertical structure has been reported in the deepest, northern inlet of BA (Medina—Gómez et al. 2014a), this stratified water mass was recorded adjacent to the northern "Punta Allen" headland, a zone which might be characterized by improved turbulence due to jet and eddy formation (Lambrechts et al. 2008). Because a variety of hydrodynamic structures may prevent vertical stratification in that area, the mere presence of such a stratification of the water column suggests that it might actually represent a more common feature than previously considered (Medina—Gómez et al. 2014a).

It is argued that physical connectivity along the whole bay and coupling between the system and the reef barrier are influenced by processes occurring over distinct time—scales, from periodic tidal oscillations to sub—tidal variability associated with wind—field forcing and atmospheric systems (Cowen et al. 2006). The ecological processes within the system may respond to such a range of astronomical and meteorological forcing, where wind stress is a major controlling factor for fish larval habitat and thus, their variability in abundance and distribution (Chiappa—Carrara et al. 2003). Furthermore, released eggs from fish spawning aggregations are prone to enter these shallow coastal systems through wind—driven flow from reproductive sites offshore (Méndez—Jiménez et al. 2015).

Additionally, far—field forcing on coastal circulation may introduce variability in the water flow of the bay and extent of exchange with the adjacent shelf sea. The system's water level responses to the near—geostrophic nature of the coastal Yucatan current (YC; Ezer et al. 2005) may influence its flushing characteristics, since the occurrence of anticyclonic eddies detached from the YC induce a barotropic pressure gradient associated with a decrease of the bay's water level and subsequent net volume displacement. Thus, under strengthened YC episodes the appearance of mesoscale eddies and their tendency to propagate into the western Caribbean Sea (i.e., getting closer to the Caribbean coastline) may couple offshore oceanographic features with ecological traits in Bahia de la Ascension by altering the flushing rates of both biologically significant particles and potentially deleterious materials (trace metals).

The presence of recurrent mesoscale oceanographic features characterizing the regional circulation pattern (e.g., Ascension—Cozumel coastal eddy; Carrillo et al. 2015) influences the residence time of particles in front of the bay (e.g., entrainment during flooding of a portion of the water mass previously carried out from the system in the last ebb tide). Thus, the dispersion of bay—directed materials might be tied to the spatial—temporal variability of this cyclonic eddy, and its persistence may induce a longer retention of outwelled materials within the gyre before they are advected offshore or more likely, northward, according to observations on the regional circulation into the coastal flow (Carrillo et al. 2015).

Finally, the current model results not only allow a better understanding of the patterns of water movement within relatively small coastal systems indented along the MBRS, but would also, if implemented as a nested model, help to improve the grasp of regional circulation by complementing information provided in mesoscale hydrodynamic studies (Ezer et al. 2005; Carillo et al. 2015). Such a nested model approach will help to examine the role of these productive ecosystems as either buffers or a source of land—derived materials to a broader area in the MBRS. This understanding is crucial to address the threat level that such inputs represent for the health of coral reef formations and the biological communities they harbor.

Conclusions

This hydrodynamic model proved to be an appropriate tool to evaluate the circulation patterns of Bahia de la Ascension under the influence of tides and winds. Tide is an important forcing function controlling the hydrodynamics of this system, as tidal phase alters both instantaneous and time—average flow in the inlet zone and the bay's central basin. Also, Trade winds acting along the northeast—southwest main—axis of the bay enhance the ocean—directed water circulation from the system's interior.

The tidally—averaged circulation is relevant for the bay's spatial heterogeneity, as it favors water exchange between the freshwater—influenced area and the marine—influenced main bay. The wind action strongly alters water exchange in BA, and the geographic orientation of the Bay aligned with the system's main axis is crucial to sustain a significant discharge through the system. The instantaneous current velocities are higher in the deeper north inlet than in the southern one, while tidally—averaged circulation showed water inflow through the latter and outflow through the north entrance.

The turnover times (T_t) in the system reflected such residual flow scenarios. The T_t length showed a correlation with the geographic orientation of the wind field, featuring shorter T_t under northeasterly winds than in north winds occurring during winter storms (*Nortes*). The influence of Trade winds constitutes a major driving force on the circulation of an embayment placed in the inner—most bay subsystem.

Acknowledgments

The authors extend their appreciation to J. Ramírez and J. Caamal of the "Primary Production" Laboratory in CINVESTAV—Unidad Mérida for their eager assistance during the field campaigns. The Nature Conservancy (TNC) and the board and staff of Reserva de la Biósfera de Sian Ka'an (National Commission of Natural Protected Areas: CONANP) provided the funds and logistics to carry out the field surveys during this study.

Literature Cited

Adame, M.F., J.B. Kauffman, I. Medina, J.N. Gamboa, O. Torres, J.P. Caamal, M. Reza, and J. Herrera—Silveira. 2013. Carbon stocks of tropical coastal wetlands within the karstic landscape of the Mexican Caribbean. PLoS ONE 8:e56569. doi:10.1371/journal.pone.0056569

Boose, E.R., D.R. Foster, A. Barker—Plotkin, and B. Hall. 2003. Geographical and historical variation in hurricanes across the Yucatan Peninsula. In: A. Gómez—Pompa, M.F. Allen, S.L. Fedick, and J.J Jiménez, eds. Lowland Maya Area: Three Millennia at the Human—Wildland Interface. Haworth Press, New York, NY, USA, p. 495—516.

Brown, C.A., S.A. Holt, G.A. Jackson, D.A. Brooks, and G.H. Holt. 2004. Simulating larval supply to estuarine nursery areas: how important are physical processes to the supply of larvae to the Aransas Pass Inlet. Fisheries Oceanography 13:181—196.

Carrillo, L., E.M. Johns, R.H. Smith, J.T. Lamkin, and J.L. Largier. 2015. Pathways and Hydrography in the Mesoamerican Barrier Reef System Part 1: Circulation. Continental Shelf Research 109:164—176. doi:10.1016/j.csr.2015.09.014.

Cavalcante, G.H., B. Kjerfve, D.A. Feary, A.G. Bauman, and P. Usseglio. 2011. Water currents and water budget in a coastal megastructure, Palm Jumeirah Lagoon, Dubai, UAE. Journal of Coastal Research 27:384—393.

Cavalcante, G.H., B. Kjerfve, and D.A. Feary. 2012. Examination of residence time and its relevance to water quality within a coastal mega—structure: The Palm Jumeirah Lagoon. Journal of Hydrology 468—469:111—119. doi:10.1016/j.jhydrol.2012.08.027.

Cetina, P., J. Candela, J. Sheinbaum, J. Ochoa, and A. Badan. 2006. Circulation along the Mexican Caribbean coast. Journal of Geophysical Research 111:1—19. doi:10.1029/2005JC003056.

Chiappa—Carrara, X., L. Sanvicente—Añorve, A. Monreal—Gómez, D. Salas De León. 2003. Ichthyoplankton distribution as an indicator of hydrodynamic conditions of a lagoon system in the Mexican Caribbean. Journal of Plankton Research 25:687—696.

Coronado, C., J. Candela, R. Iglesias—Prieto, J. Sheinbaum, M. López, and F.J. Ocampo—Torres. 2007. On the circulation in the Puerto Morelos fringing reef lagoon. Coral Reefs 26:149—163. doi:10.1007/s00338—006—0175—9.

Cowen, R.K., C.B. Paris, and A. Srinivasan. 2006. Scaling of population connectivity in marine populations. Science 311:522—527. doi:10.1126/science.1122039.

David, L.T. 1999. LOICZ budget in Laguna de Terminos, Campeche. In: S.V. Smith, J.I. Marshall, and C.J. Crossland, eds. Mexican and Central American Coastal Lagoon Systems: Carbon, Nitrogen and Phosphorus Fluxes (Regional Workshop II), LOICZ Reports & Studies No. 13, LOICZ IPO, Texel, The Netherlands, p. 9—15.

David, L.T. and B. Kjerfve. 1998. Tides and currents in a two—inlet coastal lagoon: Laguna de Terminos, Mexico. Continental Shelf Research 18:1057—1079.

Dawson, F.H. and W.N. Robinson. 1984. Submersed macrophytes and the hydraulic roughness of a lowland chalkstream. Verhandlungen Internationale Vereinigung für Theoretische und Angewandte Limnologie 22:1944—1948.

Delft3D—FLOW. 2014. Simulation of multi—dimensional hydrodynamic flows and transport phenomena, including sediments; User Manual, Version 3.15.34158. WL|Delft Hydraulics. Deltares; Delft, The Netherlands. http://www.deltares.nl.

Drew, E.A. 2000. Ocean nutrients to sediment banks via tidal jets and *Halimeda* meadows. In: E. Wolanski, ed. Oceanographic Processes of Coral Reefs: Physical and Biological Links in the Great Barrier Reef. CRC Press, Boca Raton, FL, USA, p. 255—268.

Enriquez, C., I.J. Mariño—Tapia, and J.A. Herrera—Silveira. 2010. Dispersion in the Yucatan coastal zone: Implications for red tide events. Continental Shelf Research 30:127—137. doi:10.1016/j.csr.2009.10.005.

Ezer, T., D.V Thattai, B. Kjerfve, and W. Heyman. 2005. On the variability of the flow along the Meso—American Barrier System: a numerical model study of the influence of the Caribbean current and eddies. Ocean Dynamics 55:458—475. doi:10.1007/s10236—005—0033—2.

Fernandes, E.H.L., K.R. Dyer, and L.F.H. Niencheski. 2001. TELEMAC—2D calibration and validation to the hydrodynamics of the Patos Lagoon (Brazil). Journal of Coastal Research 34:470—488.

Geyer, W.R. 1997. Influence of wind on dynamics and flushing of shallow estuaries. Estuarine, Coastal, and Shelf Science 44:713—722.

Hanshaw, B.B. and W. Back. 1980. Chemical mass—wasting of the northern Yucatan Peninsula by groundwater dissolution. Geology 8:222—224.

Hench, J.L., J.J. Leichter, and S.G. Monismith. 2008. Episodic circulation and exchange in a wave—driven coral reef and lagoon system. Limnology and Oceanography 53:2681—2694. doi: 10.4319/lo.2008.53.6.2681.

Hsu, K., M.T. Stacey, and R.C. Holleman. 2013. Exchange between an estuary and an intertidal marsh and slough. Estuaries and Coasts 36:1137—1149. doi:10.1007/s12237—013—9631—2.

Kjerfve, B. 1981. Tides of the Caribbean Sea. Journal of Geophysical Research 86:4243—4247.

Kjerfve, B. 1986. Comparative oceanography of coastal lagoons. In: D.A. Wolfe, ed. Estuarine Variability. Academic Press, New York, NY, USA, p. 63—81.

Kjerfve, B., and K.E. Magill. 1989. Geographic and hydrodynamic characteristics of shallow coastal lagoons. Marine Geology 88:187—199.

Kjerfve, B., and A.M. Oliveira. 2004. Modelling of circulation and water exchange in a hypersaline coastal lagoon: Lagoa de Araruama, Brazil. In: L. Drude de Lacerda, R.E. Santelli, E.K. Duursma, and J.J. Abrão, eds. Environmental Geochemistry in Tropical and Subtropical Environments. Springer Berlin Heidelberg, Germany, p. 235—251. doi: 10.1007/978—3—662—07060—4_18

Ladah, L., A. Filonov, M.F. Lavín, J.J. Leichter, J.A. Zertuche—González, and D.M. Pérez—Mayorga. 2012. Cross—shelf transport of sub—thermocline nitrate by the internal tide and rapid (3—6 h) incorporation by an inshore macroalage. Continental Shelf Research 42:10—19. doi:10.1016/j.csr.2012.03.010.

Lambrechts, J., E. Hanert, E. Deleersnijder, P.E. Bernard, V. Legat, J.F. Ramacle, and E. Wolanski. 2008. A multi—scale model of the hydrodynamics of the whole Great Barrier Reef. Estuarine, Coastal, and Shelf Science 79:143—151. doi:10.1016/j.ecss.2008.03.016.

Meacham, S. 2007. Freshwater resources in the Yucatan Peninsula. In: L. Holliday, L. Marin, and H. Vaux, eds. Sustainable Management of Groundwater in Mexico. The National Academies Press, Washington D.C., USA, p. 6—12.

Medina—Gómez, I. 2011. Characterization of a karst coastal ecosystem in the Mexican Caribbean: assessing the influence of coastal hydrodynamics and submerged groundwater discharges on seagrass. Ph.D. thesis. Texas A&M University, College Station, TX, USA, 101p.

Medina—Gómez, I. and J.A. Herrera—Silveira. 2009. Seasonal responses of phytoplankton productivity to water—quality variations in a coastal karst ecosystem of the Yucatan Peninsula. Gulf of Mexico Science 27:39—51.

Medina—Gómez, I., B. Kjerfve, I. Marino—Tapia, and J.A. Herrera—Silveira. 2014a. Sources of salinity variation in a coastal lagoon in a karst landscape. Estuaries and Coasts 37:1329—1342. doi: 10.1007/s 12237—014—9774—9

Medina—Gómez, I., G. Villalobos, and J.A. Herrera—Silveira. 2014b. Spatial and temporal hydrological variations in the inner estuaries of a large coastal lagoon of the southern Gulf of Mexico. Journal of Coastal Research 31:1429—1438. doi: 10.2112/JCOASTRES—D—13—00226.1.

Méndez—Jiménez, A., W.D. Heyman, and S.F. DiMarco. 2015. Surface drifter movement indicates onshore egg transport from a reef fish spawning aggregation. Physical Geography 36:353—366. doi: 10.1080/02723646.2015.1023243

Morin, J., M. Leclerc, Y. Secretan, and P. Boudreau. 2000. Integrated two—dimensional macrophytes—hydrodynamic modeling. Journal of Hydraulic Research 38:163—172.

Murphy, A. 1988. Skill scores based on the mean square error and their relationships to the correlation coefficient. Monthly Weather Review 116:2417—2424.

Nixon, S.W. 1988. Physical energy inputs and the comparative ecology of lake and marine ecosystems. Limnology and Oceanography 33:1005—1025.

Pawlowicz, R., B. Beardsley, and S. Lentz. 2002. Classical tidal harmonic analysis including error estimates in MATLAB using T_TIDE. Computers and Geosciences 28:929—937.

SMN, 2007. Servicio Meteorológico Nacional de México (Datos históricos EMAs). http://smn.cna.gob.mx/productos/emas/emas.html. (Viewed on 11/11/2011).

Sousa, M.C. and J.M. Dias. 2007. Hydrodynamic model calibration for a mesotidal lagoon: the case of Ria de Aveiro (Portugal). Proceedings of the 9th International Coastal Symposium. Journal of Coastal Research, Special Issue No. 50:1075—1080.

Staneva, J.V. and E.V. Stanev. 1998. Oceanic response to atmospheric forcing derived from different climatic data sets. Intercomparison study for the Black Sea. Oceanologica Acta 21:393—417.

Sutherland, J., D.J.R. Walstra, T.J. Chesher, L.C. van Rijn, and H.N. Southgate. 2004. Evaluation of coastal area modelling systems at an estuary mouth. Coastal Engineering 51:119—142. doi:10.1016/j.coastaleng.2003.12.003.

Taebi, S., R.J. Lowe, C.B. Pattiaratchi, G.N. Ivey, G. Symonds, and R. Brinkman. 2011. Nearshore circulation in a tropical fringing reef system. Journal of Geophysical Research 116:C02016. doi:10.1029/2010JC006439.

Thattai, D., B. Kjerfve, and W.D. Heyman. 2003. Hydrometeorology and variability of water discharge and sediment load in the inner Gulf of Honduras, western Caribbean. Journal of Hydrometeorology 4:985—995. doi:10.1175/1525—7541(2003)004<0985:HAVOWD>2.0.CO;2.

Tilburg, C.E., S.M. Gill, S.I. Zeeman, A.E. Carlson, T.W. Arienti, J.A. Eickhorst, and P.O. Yund. 2011. Characteristics of a shallow river plume: observations from the Saco River Coastal Observing System. Estuaries and Coasts 34:785—799. doi:10.1007/s12237—011—9401—y

Umgiesser, G. and R. Neves. 2005. Physical processes. In: I.E. Gönec and J.P. Wolflin, eds. Coastal Lagoons: Ecosystem Processes and Modeling for Sustainable Use and Development. CRC Press, Boca Raton, FL, USA, p. 43—78.

Walstra, D.J.R., L.C. Van Rinj, H. Blogg, and M. Van Ormondt. 2001. Evaluation of a hydrodynamic area model based on the Coast3D Data at Teignmouth 1999. Proceedings of the Fourth Conference on Coastal Dynamics, Lund, Sweden, (11—15 June 2001), American Society of Civil Engineers, ISBN 0784405662, p. D4.1—D4.4.

Wolanski, E. 1994. Physical Oceanographic Processes of the Great Barrier Reef. CRC Press, Boca Raton, FL, USA, 194 p.